ISBN: 978-3-95450-201-1 doi:10.18429/JACoW-IBIC2018-MOPA09

OVERVIEW OF BEAM INSTRUMENTATION AND COMMISSIONING RESULTS FROM THE COHERENT ELECTRON COOLING EXPERIMENT AT BNL*

T. A. Miller†, J. C. Brutus, W. Dawson, D. M. Gassner, R. Hulsart, P. Inacker, J. Jamilkowski, D. Kayran, V. N. Litvinenko[1], C. Liu, R. Michnoff, M. Minty, P. Oddo, M. Paniccia, I. Pinayev, Z. Sorrel, J. Tuozzolo, C-AD, BNL, 11973 Upton, NY, USA
[1] also at Department of Physics and Astronomy, SBU, 11794, Stony Brook, NY, USA

Abstract

The Coherent Electron Cooling (CeC) Proof-of-Principle experiment [1], installed in the RHIC tunnel at BNL, has completed its third run. In this experiment, an FEL is used to amplify patterns imprinted on the cooling electron beam by the RHIC ion bunches and then the imprinted pattern is fed back to the ions to achieve cooling of the ion beam. Diagnostics for the CeC experiment have been fully commissioned during this year's run. An overview of the beam instrumentation is presented. This includes devices for measurements of beam current, position, profile, bunch charge, emittance, as well as gun photocathode imaging and FEL infra-red-light emission diagnostics. Design details are discussed and beam measurement results are presented.

INTRODUCTION

During CeC's operation this year [2], its complete array of instrumentation proved useful in measuring the parameters of the 1.5 MeV electron beam, with bunch charges of 50 pC – 5 nC, 10 – 500 ps long, produced by the CeSb 112 MHz SRF Photoinjector and transported through the 704 MHz SRF 5-cell Linac [3]. The 15 MeV accelerated beam passes into the RHIC common section through the modulation drift section, undulator (or wiggler) amplification section, and kicker drift section before being diverted down the extraction line into the high-power aluminium beam dump, as shown in the layout in Fig. 1. Pulsed beam operation ran at a 1 Hz rate with trains of pulses spaced at 78 kHz (the RHIC revolution frequency).

The transport is equipped with differential current transformers and beam position monitors with positions alarms that provide the two primary machine protection measures. Plunging YAG:Ce profile monitors measure beam profile with a multi-slit mask in the injection section to measure emittance. The high power and low power beam dumps are isolated to measure beam charge. The gun is equipped with cathode imaging optics in conjunction with the laser delivery system. Infrared (IR) emission from the undulators is characterized by an IR optics instrument array [4] beneath a diamond viewport in the RHIC beamline downstream of the CeC experiment.

BEAM CURRENT AND CHARGE

In order to display and log the charge in the electron bunch, beam current can be collected in one of two beam dumps and is measured in two integrating current transformers (ICT).

Faraday Cups

The two beam dumps in the beamline are electrically isolated to function as Faraday Cups (FC) to collect and measure the beam charge. These are the high-power beam dump at the end of the CeC transport and the low power dump at the end of the injection straight section. They are connected by ¼"-Heliax cable to integrating charge amplifiers located outside the tunnel to measure the collected charge and display in pC with an update rate of 1Hz. The FC's are terminated in the tunnel each with a 10 MΩ resistor and a 1nF capacitor. The signals are brought to a multiplexer for monitoring the signal on an oscilloscope or to be digitized. The majority of operations were made with the signals going to the oscilloscope.

Temperature The thermal mass of the high-power beam dump is fitted with two rad-hard thermocouples. The low power beam dump is fitted with an RTD-type probe. These probes are monitored by analog type 4-20 mA thermocouple transmitters mounted near the beam dumps. The thermocouple, made by Okazaki [5], is an AEROPAK

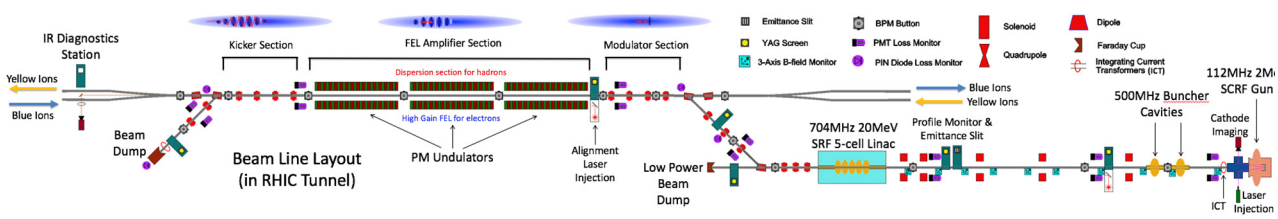

Figure 1: CeC beam line layout as installed at the 2 O'clock interaction point it the RHIC tunnel.

*Work supported by U.S. DOE under contract No DE-AC02-98CH10886 with the U.S. DOE
†tmiller@bnl.gov

ISBN: 978-3-95450-201-1 doi:10.18429/JACoW-IBIC2018-MOPA09

model, composed of a Type-K ungrounded hot junction, surrounded by MgO insulation packed in a thin Inconel tube, with a mini-plug termination. This plugs into a nearby chassis containing FlatPak series 250T analog 4-20 mA transmitters, by Acromag [6]. This model was chosen for its all analog design for increased radiation hardness.

Integrating Current Transformers

Beam charge is non-destructively measured by two ICT type in-flange integrating current transformers from Bergoz. These are mounted, one just after the gun and one just before the beam dump. Both ICTs have a 1.25 Vs/C sensitivity

The two ICTs provide independent signals for instrumentation and provide differential signals for machine protection. The beam pulse charge is reported for every pulse and a charge difference between ICTs is provided as an input the Machine Protection System (MPS). Charge calculation occurs on every pulse and the array represents all the charge values captured in 1 second. Average current is reported as the quotient of average charge and average pulse rate.

In lieu of using the typical Integrate-Hold-Reset electronics from Bergoz, the ICT signals are digitized directly. To increase the sensitivity and signal to noise ratio of the ICTs, two amplifiers are installed for each ICT. The output is buffered to both a digitizer and an oscilloscope.

Digitization

The ICT pulses are digitized with continuous acquisition and analysis without the need of an external trigger. The digitizer, referred to as the "Zynq" module, is based on the Xilinx Zynq proto-type module combined with a 4DSP FMC112 analog front end. ICT pulses are sampled at a max rate of 125 MHz with a 14-bit ADC. For every pulse, the Zynq integrates and calculates charge and performs a difference calculation. It uses the pulse charge information to determine the beam current and uses the differential measurements for beam efficiency calculations for the MPS.

Zynq Processing Description The charge is determined by integrating the raw signals from the ICTs. The integration is performed in two steps, first an integration window is specified followed by a baseline window, with indexes specified by the user. Integration calculations are performed on the upstream and downstream ICTs and the maximum instantaneous value is saved. Integral values are scaled and truncated to 16 bits and stored in DPRAM at a decimated rate (up to 32K samples) for display. When operating with a high number of pulses, the decimation rate must be increased in order to capture all the pulses. The integral values are also sent to a running average block, where a new variable length average is computed and displayed for each entry. The latency is approximately 8 nsec per the number of samples in average.

A one-second sum is computed, with a similar latency, for the integral data with a period based on the number of clocks in the average. The periodic timed sums are compared continuously to high maximum and low maximum alarm thresholds with single error thresholds and reported to the MPS. The total losses are calculated as the difference of the scaled integrals for the upstream and downstream ICTs and saved in a data array. A periodic timed sum is computed from the difference of the two scaled integrals. This sum is continuously compared to a maximum alarm threshold with a single error threshold and reported to the MPS.

The faraday cup signals are terminated locally with 1MΩ and transported out of the RHIC tunnel to amplifiers in the instrumentation racks. These signals are then passed to the Zynq and are integrated using the same algorithm described for the ICTs.

Charge Build-up

During the second year of operation, cumulative drifting of the electron beam was observed with fast returns to the original orbit along with a current spike in the ICT having a regular periodicity of about 17 minutes during pulsed beam operation at 1 Hz with pulse trains of 57 pulses of 200pC/pulse @ 78 kHz, (11.4 nA average current). This behavior is indicative of charge buildup on the ceramic and diverting the beam. A new ICT was ordered with an arbitrary aperture option, reducing the aperture to 60mm to hide the ceramic behind a 1-mm gap. This was installed for the second year of operation and this behavior was no longer observed.

Recent ICT Failure

During the 2017 run, the ICT installed in the extraction line failed to produce a signal on June 21, just before the end of the run. The ICT was removed during the following shutdown and replaced with the ICT from the CeC gun, that was replaced by the new shielded version.
It was known that in preparation of the 2017 run, this ICT was over baked to 188C, 38C over the 150C temperature limit. As the Zynq was used for direct digitization, the calibration coefficient was changed to match the gun and dump ICT responses. This ICT functioned properly from April – the beginning of the run – until it failed on June 21. Upon inspection of the ICT by Bergoz, the only failure that was found was a decrease in core permability, typically caused by over temperature. It was not discovered why the ICT continued to function after the over temperature incident, nor why it suddenly failed to operate. Radiation monitors were later installed nearby to monitor dose rates near the dump for increased protection of the hardware.

BEAM POSITION

There are 12 button-style BPM pick-ups installed in the beam transport. These are attached with ¼" Heliax phase stabilized cable to 4-channel Libera [7] Single Pass E electronic modules installed in three 4-module chassis. Two additional four-button stations are mounted upstream and downstream of the CeC transport common to the RHIC ion beams for ion beam position measurement. These are connected to a fourth chassis with two Libera Single Pass H electronic modules installed. The electron beam position must be measured independently of the ion beam. This is possible while operating in background mode where the

ISBN: 978-3-95450-201-1 doi:10.18429/JACoW-IBIC2018-MOPA09

electron bunch is injected into the RHIC abort gap without overlapping with the ion bunch. During this mode, the electron bunch is injected in the middle of the RHIC abort gap. Thus, the electron BPM's are triggered with the electron bunch, about 400 ns after the last ion bunch, and the ion BPM's are triggered with the ions, about 400 ns after the electron bunch for independent position measurements.

Position data logged during operations that shows a 200um peak to peak variation is in line with a 30 – 40 μm rms standard deviation of position.

BEAM PROFILE

A total of six beam profile monitors are installed in the transport. All consist of scintillating screens made of 30 mm diameter monolithic YAG:Ce crystals mounted normal to the beam, with a polished copper mirror behind for viewing by the camera optics. This arrangement provides an optical viewing area of 25 mm in diameter. To bleed off charge, the upstream face of the YAG crystal is coated with 100nm of aluminum. The YAG & mirror assemblies are inserted into the beam path by pneumatic actuators mounted on the top port of a six-way cross. The pneumatic actuators can be replaced without breaking vacuum.

Commissioning experience from the first year's run led to the design and installation of impedance limiting shields that slide up and down in the vertical bore to block off the transverse horizontal bore, including conical transitions in the bore for the optical viewport.

Optics

Cameras with Gigabit Ethernet (GigE) interface were chosen for the simplest infrastructure. All cameras connect to a private network switch shared only by the video server. The video server has a second network interface card (NIC) to interface with the department network for serving images published by the software manager running on the server. The Prosilica GT1600 model camera, from Allied Vision Technologies (AVT) was chosen for its integrated lens p-iris control; which is a new type of stepper motor driven iris control that can be set and maintained through power cycles. The camera has a 1/1.8-type 2MP sensor with a wide gain of 0 – 26 dB. Its external trigger is synchronized to the electron beam and its exposure times range from 10us to 68.7 sec. It is paired with a 50mm lens, Edmund Optics (EO) model 89-938, having a stepper motor driven iris with apertures of f/2.1 to f/95 in 42 increments. During bench tests the optical resolution was determined to be < 50 μm by the measured contrast, or modulation transfer function (MTF) > 27 % from a 10 line-pairs/mm resolution target.

A white LED ring on the face of the optical viewport illuminates the in-vacuum view to check the health of the screen. As a focusing aid, a 450nm blue laser is used to excite the YAG crystal. It is injected into the optical axis using a dichroic beam splitter (EO 69-899), 1mm thick with a 500nm cut-on, placed in front of the lens. This also blocks the laser light from the camera while allowing most of the YAG emission to pass through to the camera. For increased structure in the laser induced pattern, on which to focus, on the crystal, a diffractive optical element, model D-ER-340 from Holoeye Photonic [8], diffracts the laser spot into a chopped cross pattern that is centered on the YAG screen.

EMITTANCE

A multi-slit mask is installed in the injection section upstream of a profile monitor. It is inserted with a three-position pneumatic actuator with two insertable positions for horizontal and vertical slits and can be fully retracted from the beam aperture. The slit mask, as shown on the right in Fig. 2, with dimensions tailored for the expected beam divergence, was made of 1mm-thick tungsten having 10 slits that were wire-EDM cut to be 200 μm wide, spaced 2 mm apart, for both the horizontal and vertical positions.

The incoming beam is sampled by the multi-slit mask, as shown on the left in Fig. 2, where the effect of space charge is removed and the new beamlets propagate to the downstream profile monitor. The image of the beamlets is analyzed by an algorithm [9] developed at BNL to fit a multi-gaussian shape to the beamlets' profiles. The average divergence of each beamlet is calculated based on slit positions and gaussian peak positions. The rms divergence of beamlets are calculated from the rms of gaussian peaks. The emittance is then calculated from the position angle correlation and the rms divergence of the beamlets.

Special features are built into the image capture software so that a region of interest can be selected through the beamlets' projection and a resulting profile is generated, calibrated in mm instead of pixels. The user specifies the parameters of slit width, slit spacing, drift length, scaling factor, and angle of rotation. A multi-gaussian fit is performed and displayed with measurements of amplitude, sigma, and peak locations that are processed by an add-on algorithm to calculate the beam emittance.

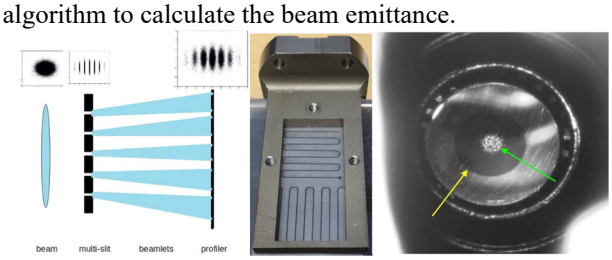

Figure 2: Left: Schematic of mulit-slit emittance measurement, Middle: photo of tungsten mask in SS holder, Right: Image of polished molybdenum cathode puck surface. The dark circle (yellow arrow) is the 12 mm diameter activated cathode area. The bright spot in the center (green arrow) is the laser spot.

GUN PHOTOCATHODE IMAGING

The surface of the polished molybdenum puck, with the activated cathode area, in the superconducting RF photoinjector is imaged, as shown in Fig. 2, for use during cathode insertion and alignment as well as for imaging the laser spot on the cathode surface and checking the health of the cathode surface. The camera with illumination assembly is mounted in the laser exit table enclosure, 1.30 m downstream of the cathode, and uses the laser exit mirror

ISBN: 978-3-95450-201-1 doi:10.18429/JACoW-IBIC2018-MOPA09

to view the cathode. A 2 MP GigE camera, AVT model Manta G201B, is fitted with a Navitar 6x ZoomXtender [10] lens assembly (working distance of 0.3 – 16 m) to overcome the long distance and limited aperture. Illumination of the cathode is made by a high power collimated single-die white LED with 800mW of output. This lamp illuminates on-axis with the optical path of the camera through a 50:50 UV Fused Silica broadband plate beam splitter. Nuisance reflections off of in-vacuum aperture limiting surfaces caused glare that bloomed into the image. This was mitigated by a spotlight arrangement with the LED mounted to dual condenser lenses around an iris, adjusted to focus the smallest spot through the limiting aperture to reduce the glare.

FEL INFRA-RED-LIGHT EMISSION DIAGNOSTICS

Light emitted from the undulators in the "amplifier section" is detected and analyzed as a feedback of both the position of the electron beam in the wiggler as well as the degree of overlap of the electron and ion beams. An increase in emission power is expected to indicate the onset of coherent amplification in the undulators. The profile of the emission pattern will be a function of the angular trajectory through the undulators. In order to provide data on these parameters, an array of optical instruments is installed downstream of a RHIC DX magnet under an optical viewport where a copper mirror plunges in to extract the undulator light between the separated RHIC ion beams. All optics were designed to have a 50 mm aperture.

Although the experiment was designed for 21.8 MeV, giving an IR emission at 14 μm, the 704 MHz SRF 5-cell Linac was operated at reduced energy during this year's run. The resulting final beam energy of 15 MeV resulted in a shift of the expected undulator emission to 30 μm. The ZnSe viewport was replaced with a CVD diamond viewport to transmit the longer wavelength as well as a green alignment laser, injected upstream of the undulators. The IR detectors were changed to Terahertz band detectors.

Power

In order to cover an optical power range wide enough to detect down to 10 nW from spontaneous emission and measure up to 3W during coherent amplification, three different detectors were used, as summarized in Table 1.

Three remote controlled flip mirrors are used to divert the light between detectors, as shown in the optics layout in Fig. 3. The 3A Thermoelectric detector has a slow 2.5 s response to CW light; whereas, the THZ5I Pyroelectric detector and Golay Cell require a chopped signal, provided by the chopper wheel. A thermal source is included with its own flipper mirror for an on-board test.

Table 1. Summary of IR Detectors

Detector (mfgr)	Range	Chop
3A-P-THz (Ophir)	15 μ – 3 W	DC
Golay Cell (Tydex)	10 n – 10 μW	15 Hz
THZ5I (Gentech)	10 n – 128 μW	5 – 25 Hz

Profile

A scanning pinhole, moved by two X-Y stepper motor drivers orthogonal to the light path, is scanned in a raster pattern over a user selectable area while the Golay Cell response is digitized to build an array of data that is assembled into an image with interpolation between points. With the iris set to 4 mm, a full scan of the 50mm beam is made with 20 horizontal lines (2.5 mm apart for a 50 x 50 mm scan) takes about 3 minutes to complete. The image building routine is embedded in our versatile profile monitor image viewing software.

Spectrum

The wavelength of the undulator emission is proportional to the absolute energy of the electron beam; which much be matched closely to the ion beam it will cool. A monochromator, model SP2150I from Princeton Instruments [11], is used to measure the emission wavelength. It has a mirror and a 30 μm grating installed on s grating selection turret. The mirror is selected to pass all light during optical alignment. The wavelength of the undulator light was effectively measured at 31.2 μm.

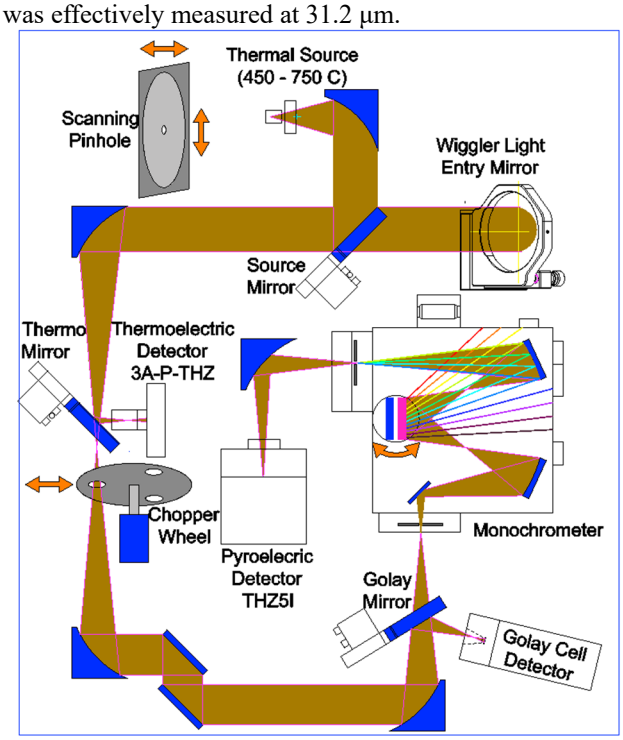

Figure 3: IR Optics layout.

BEAM LOSS

A system to monitor beam losses during commissioning and tuning is installed but not connected to the MPS. There are seven beam loss monitor stations with loss monitors mounted on beam left and beam right (14 channels total). The detectors are photomultiplier tubes (PMT) mounted in light-tight housings with a test LED inside, fashioned after those used for the 12 GeV upgrade to CEBAF [12] at JLAB. The signals from the PMTs will be processed by VME based 8-channel FPGA electronics cards [13] purchased from JLAB. With a 1-μs fast shutdown output to

ISBN: 978-3-95450-201-1 doi:10.18429/JACoW-IBIC2018-MOPA09

the MPS, this PMT BLM card also has a parallel log amplifier signal path to provide 5 decades of dynamic response to aid in tuning of the machine with low power beam to reduce losses.

STRAY MAGNETIC FIELDS

The energy of the electron beam was low enough for stray fields from the nearby RHIC magnets to deflect the beam. It was found during the first year of commissioning that these fields were difficult to compensate for with correctors. Thus, a series of 3-axis fluxgate magnetometers were installed, namely Watson Industries model FGM-301 [14]. A total of 10 units, with a range of ±700 mGauss, were installed in the low energy section between the gun and the Linac

ACKNOWLEDGEMENTS

The authors would like to thank J. Tuozzolo, Cliff Brutus, G. Mahler and other members of the engineering & design team, and M. Mapes, and other members of the Vacuum Group, and M. Harvey and other members of the Controls Group, and T. Curcio and D. Lehn and other members of the Accelerator Components & Instrumentation Group.

REFERENCES

[1] V. Litvinenko, et al "Proof-of-Principle Experiment for FEL-Based Coherent Electron Cooler", in *Proc. FEL2011*, Shanghai, China, 2011, paper WEOA3

[2] V. Litvinenko, et al "Status of Proof of Principle Experiment of Coherent Electron Cooling at BNL", in *Proc. COOL'17*, Bonn, Germany, 2017, paper WEM22

[3] I. Pinayev, et al, "Coherent Electron Cooling Diagnostics: Design Principles and Demonstrated Performance", presented at the 7th Int. Beam Instrumentation Conf. (IBIC'18), Shanghai, China, Sept 2018, paper TUOB01, this conference

[4] T. Miller, et al "Infrared Diagnostics Instrumentation Design for the Coherent Electron Cooling Proof of Principle Experiment", in *Proc. FEL'14*, Basel, Switzerland, Aug 2014, paper THP074

[5] Okazaki Manufacturing Company, https://www.okazaki-mfg.com/en/BasicProducts/Aeropak.html

[6] Acromag, https://www.acromag.com

[7] Instrumentation Technologies, https://www.i-tech.si/

[8] Holoeye Photonics, https://holoeye.com/diffractive-optics/

[9] C. Liu, et al., "Multi-slit based emittance measurement study for BNL ERL" in *Proc. IPAC'13*, Shanghai, China, May 12-17, 2013, paper MOPWA083

[10] Navitar, https://navitar.com/products/imaging-optics/high-magnification-imaging/zoom-6000/

[11] Princeton Instruments, https://www.princetoninstruments.com

[12] J. Perry, et al., "The CEBAF Beam Loss Sensors", in *Proc. PAC'93*, Washington DC, May 1993, pp 2184 - 2186

[13] J. Yan and K. Mahoney, "New Beam Loss Monitor for 12 GeV Upgrade", in *Proc. ICALEPCS'09*, Kobe, Japan, Oct. 2009, paper WEP092

[14] Watson Industries, http://watson-gyro.com/product/magnetometers/fluxgate-magnetometer-fgm-301/